THE JOURNAL OF PHYSICAL CHEMISTRY Letters

Letter

pubs.acs.org/JPCL

Pressure-Dependent Light Emission of Charged and Neutral Excitons in Monolayer $MoSe_2$

Xinpeng Fu,[†] Fangfei Li,[*,†] Jung-Fu Lin,[‡] Yuanbo Gong,[†] Xiaoli Huang,[†] Yanping Huang,[†] Bo Han,[†] Qiang Zhou,[*,†] and Tian Cui[†]

[†]State Key Laboratory of Superhard Materials, College of Physics, Jilin University, Changchun 130012, China

[‡]Department of Geological Sciences, The University of Texas at Austin, Austin, Texas 78712, United States

Supporting Information

ABSTRACT: Tailoring the excitonic properties in two-dimensional monolayer transition metal dichalcogenides (TMDs) through strain engineering is an effective means to explore their potential applications in optoelectronics and nanoelectronics. Here we report pressure-tuned photon emission of trions and excitons in monolayer $MoSe_2$ via a diamond anvil cell (DAC) through photoluminescence measurements and theoretical calculations. Under quasi-hydrostatic compressive strain, our results show neutral (X^0) and charged (X^-) exciton emission of monolayer $MoSe_2$ can be effectively tuned by alcohol mixture vs inert argon pressure transmitting media (PTM). During this process, X^- emission undergoes a continuous blue shift until reaching saturation, while X^0 emission turns up splitting. The pressure-dependent charging effect observed in alcohol mixture PTM results in the increase of the X^- exciton component and facilitates the pressure-tuned emission of X^- excitons. This substantial tunability of X^- and X^0 excitons in $MoSe_2$ can be extended to other 2D TMDs, which holds potential for developing strained and optical sensing devices.

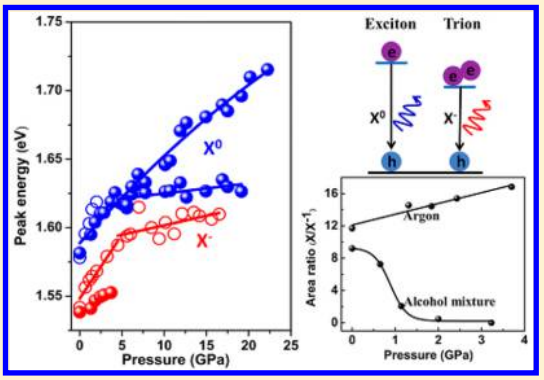

Atomically thin transition metal dichalcogenides (TMDs) 2H-MX_2 (M = Mo, W, and etc.; X = S, Se, and Te) have attracted widespread attention owing to their unusual optical and electronic properties.[1−6] The fundamental optical excitation of semiconductors is an exciton (X^0) associated with the Coulomb-bound excited electron and hole. Trions can be formed by extra capture of one electron or hole when the Coulomb interaction is strong enough. The latter term divides into two states: two electrons and one hole correspond to a negatively charged trion (X^-), and one electron and two holes correspond to a positively charged trion (X^+). Binding energies of excitons and trions in 2D TMDs are as high as a few hundred meV, which is an order of magnitude larger than conventional semiconductor quantum wells. This property originates from the large carrier effective masses, strong quantum confinement, and reduced dielectric screening due to the monolayer thickness.[7−10] Strong Coulomb interactions make these quasiparticles stable at room temperature and relevant for optoelectronic devices.[11−15] As a consequence, monolayer TMDs have potential applications in controllable 2D electronic systems. Recently, increasing attention is being paid to their excitonic physics including interexcitonic scattering,[16] exciton-carrier broadening,[17,18] biexciton formation,[19] as well as exciton valley relaxation dynamics.[20]

$MoSe_2$, a member of the group-VI TMDs, is composed of a single layer of Mo atoms covalently bonded between two laminar sheets of Se atoms. Monolayer $MoSe_2$ has a direct band gap at the K points in the first Brillouin zone. The emission of X^0 and X^- excitons generated by the direct interband transition at room temperature has been observed in previous reports. Their well-separated excitonic features possess advantages for exploring excitonic physics. Recently, electrical control of the excitonic species among positively charged (X^+), neutral (X^0), and negatively charged (X^-) excitons of monolayer $MoSe_2$ has been achieved using a back-gated field-effect transistor (FET) device.[7] By setting V_g to be negative or positive, X^0 excitons were turned into X^+ or X^- excitons, respectively. On the other hand, strain engineering via application of hydrostatic pressure has been shown to be an effective means to modulate electronic band gaps and charges in monolayer MoS_2, heterostructured MoS_2, and graphene. The direct band gap increased from 1.85 to 2.08 eV when the monolayer MoS_2 was exposed over a pressure range of 0−16 GPa.[21] *p*-Type doping of graphene was observed in graphene/MoS_2 heterostructures due to the charge transfer and reached a doping concentration of ~3.2 × 10^{13} cm^{-2} at 30 GPa.[22] These studies have demonstrated that strain engineering is an important routine to control behaviors of excitons and trions. More importantly, the strain-induced charging effect enables simultaneous tuning of the content and energy of excitons and trions in monolayer 2D TMDs, which holds potential for light-emitting device applications.[23,24]

Received: June 1, 2017
Accepted: July 17, 2017
Published: July 17, 2017

DOI: 10.1021/acs.jpclett.7b01374
J. Phys. Chem. Lett. 2017, 8, 3556−3563

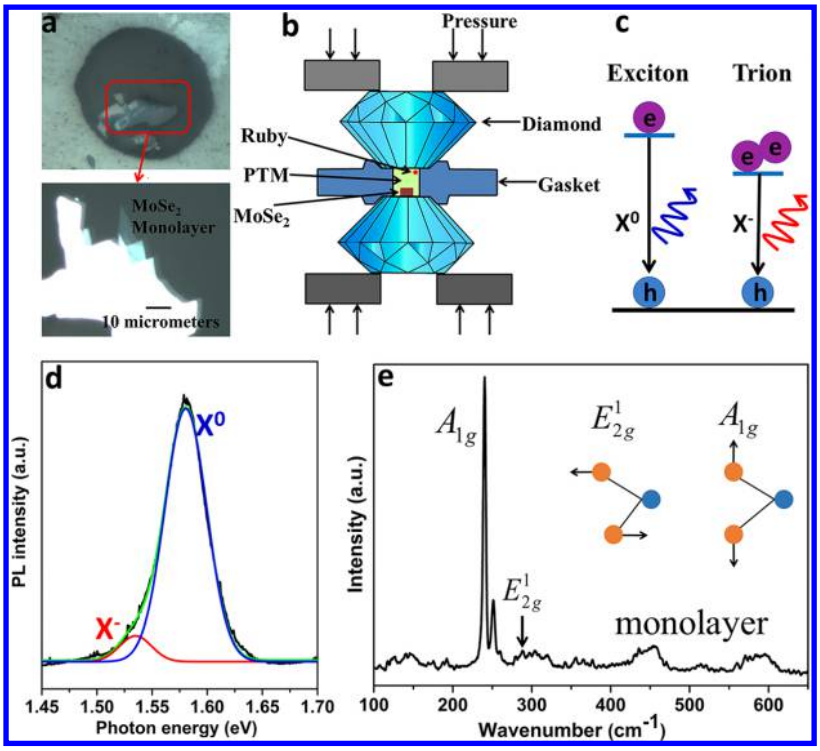

Figure 1. (a) Representative photo of the monolayer $MoSe_2$ placed in the sample chamber of the DAC in alcohol mixture PTM. The photo of the monolayer 2H-$MoSe_2$ film shown in the red box is enlarged in the image below. The sample can be easily distinguished in an optical microscope with its distinct optical contrast (lower figure). (b) Schematic diagram of the DAC for PL and Raman experiments. (c) Illustration of the transition processes for neutral (X^0) and charged (X^-) excitons in monolayer 2H-$MoSe_2$. (d) PL spectrum of monolayer 2H-$MoSe_2$ at ambient conditions. The neutral exciton emission (blue curve) is very dominant, while the charged exciton (red curve) is weak at ambient conditions. (e) Raman spectrum of monolayer 2H-$MoSe_2$ at ambient conditions. The insets show the normal vibrational modes of monolayer 2H-$MoSe_2$. Blue and orange circles represent Mo and Se atoms, respectively.

In this work, we report the first study on effective tuning of exciton and trion emission of the exfoliated monolayer $MoSe_2$ via hydrostatic pressure and charging effects using photoluminescence (PL) spectra in a diamond anvil cell (DAC) loaded with argon or alcohol mixture pressure transmitting media (PTM). We found a pressure-dependent charging effect in alcohol mixture PTM, which led to the increase of the X^- exciton component and facilitated the emission of X^- excitons being modulated continuously to high pressure. Meanwhile, the tunability of X^0 emission at high pressure can be achieved by employing argon as PTM. At low pressure, the energies of X^- and X^0 emission exhibit an approximately similar blue shift rate, and then X^- emission gradually reaches saturation, whereas pressure-induced splitting of X^0 emission appears at high pressure. The obtained strain-related response of X^0 and X^- exciton emission in monolayer $MoSe_2$ in a controlled environment is helpful for developing strained $MoSe_2$ devices. In addition, the ability of switching between these two distinctly different pressure-dependent evolutions of the PL spectrum by controlling the contents of X^0 and X^- excitons is significant for optoelectronic applications.

Monolayer 2H-$MoSe_2$ film was prepared by mechanically exfoliating a $MoSe_2$ single crystal (2D Semiconductor Supplies, USA) using GEL film (Gel-Pak).[25,26] The monolayer $MoSe_2$ was transferred onto a diamond anvil surface, which also served as the substrate in the sample chamber. Regions of monolayer $MoSe_2$ were identified by their optical contrasts with the background using an optical microscope. Further confirmation was followed by employing PL measurements (Figure 1d) and Raman spectra measurements (Figure 1e). The DAC device provides hydrostatic pressure, and its schematic diagram is shown in Figure 1b. The top-view microscope image of the pressure chamber is exhibited in Figures 1a and S1. Two different types of PTMs, argon and alcohol mixture, were used in this work. The optical response of monolayer $MoSe_2$ is dominated by excitonic transitions. As illustrated in Figure 1c, the emission of X^0 and X^- excitons originates from the transition of Coulomb-bound electron−hole and 2electron−hole quasiparticles in the band gap, respectively, and the emission of X^- excitons red shifts from the X^0 excitons.

Figure 1d shows the typical PL spectrum of a monolayer $MoSe_2$ at ambient conditions, which has been well fitted using two Gaussian functions. The two fitted peaks, a small one located at the lower energy side and a main broad peak located at the higher energy side, are assigned to negatively charged exciton X^- (at 1.54 eV) and neutral exciton X^0 (at 1.58 eV) emission, respectively, which is in agreement with previous reports.[7,27−30] The existence of X^- emission suggests an unintentional doping effect related to the structural defects.[31−33]

The Raman spectrum of bulk 2H-$MoSe_2$ is shown in Figure S2, and the vibrational normal modes are illustrated in the inset. Four normal vibrational modes were studied in bulk 2H-$MoSe_2$, including B_{2g}^1 at 351.03 cm^{-1}, E_{1g} at 169.77 cm^{-1}, E_{2g}^1 at 284.5 cm^{-1}, and A_{1g} at 242.02 cm^{-1}. The E_{1g}, E_{2g}^1, and A_{1g} modes originate from the in-plane vibration of Se−Se atoms, in-plane vibration of Mo−Se atoms, and out-of-plane vibrations of Se−Se atoms in opposite directions, respectively. The B_{2g}^1 mode is expected to be present in multilayer $MoSe_2$ because it arises from out-of-plane (breathing) vibration and has been used as

DOI: 10.1021/acs.jpclett.7b01374
J. Phys. Chem. Lett. 2017, 8, 3556−3563

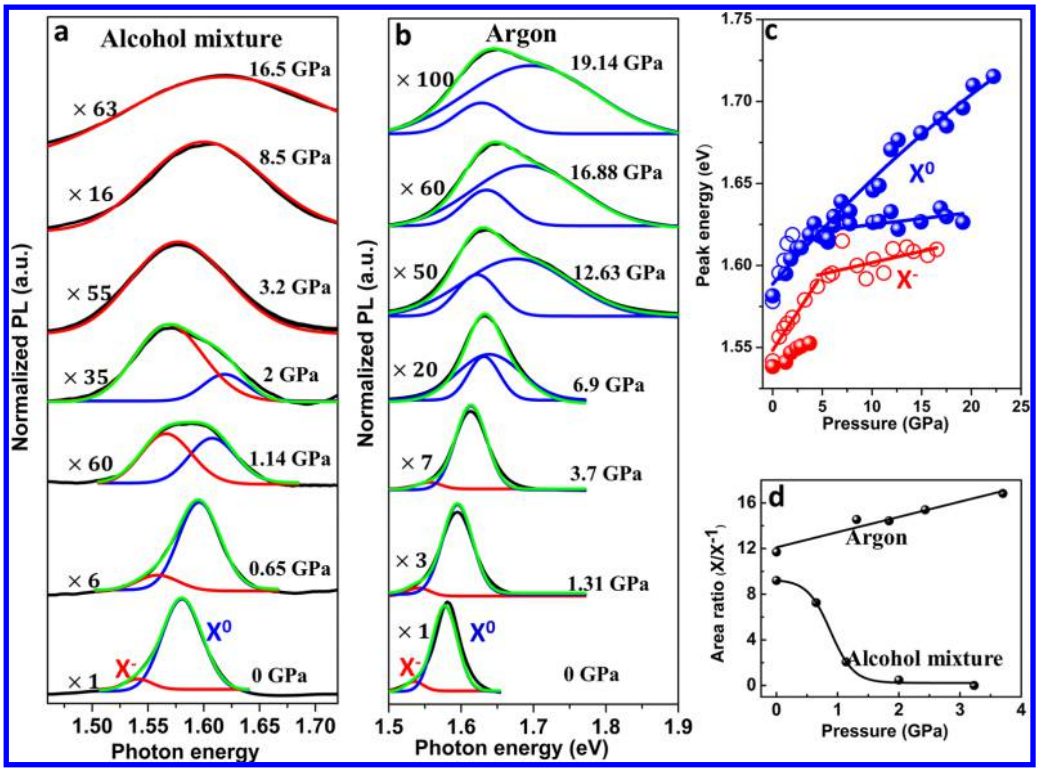

Figure 2. (a) PL spectra of monolayer 2H-$MoSe_2$ immersed in alcohol mixture PTM at high pressure. (b) PL spectra of monolayer 2H-$MoSe_2$ in argon PTM at high pressure. The spectra are normalized to show characteristic features at high pressure. Panels (a) and (b) show experimental spectra (black lines) with spectral fits to X^0 exciton emission (blue lines), X^- emission (red line), and overall fitted spectra (green lines). (c) Peak energy evolution of PL peaks fitting as a function of pressure in two PTM. Solid circles represent X^- (red ●) and X^0 (blue ●) excitons in argon PTM, and hollow circles represent X^- (red ○) and X^0 (blue ○) excitons in alcohol mixture PTM. (d) Pressure-dependent area ratio of exciton/trion (X^0/X^-) versus pressure.

an important criterion in distinguishing the monolayer from multilayers. In our monolayer $MoSe_2$, intense A_{1g} peaks are observed, and the $B_{2g}{}^1$ mode is not observed as expected (Figure 1e). When the bulk was thinned to a monolayer, a 1.8 cm^{-1} red shift of the A_{1g} mode and a 3.83 cm^{-1} blue shift of the $E_{2g}{}^1$ mode were observed because of the competition between surface effects and thickness effects,[34] which are consistent with the previous results.[27,35,36]

After confirming that the prepared sample was indeed monolayer 2H-$MoSe_2$, the pressure-dependent PL measurement was conducted using alcohol mixture PTM, and the normalized PL spectra of monolayer $MoSe_2$ are presented in Figure 2a. The scaling factors for the normalization are listed on the left side of the corresponding curves, and a larger factor corresponds to a smaller PL intensity. The raw data in Figure 3a were fitted with a multi-Gaussian function, and individual component X^0 and X^- emission is displayed in blue curves and red curves for pressures of 0 GPa and above. As the pressure increases, both X^- and X^0 peaks exhibit blue shifts, but the relative intensity evolutions give an obvious contrary transition. The integrated intensity of the X^- peak tended to increase with pressure, while that of the X^0 peak showed the opposite trends. When the pressure was increased to 3.2 GPa, the neutral exciton X^0 peak disappeared, leaving the X^- peak to become the main emission. Then, with further compression, the X^- emission vanished above 16.5 GPa. The unusual behaviors of PL have never been observed in any previous study of pressure-tuning monolayer TMDs and present a pressure-enhanced charging effect in monolayer $MoSe_2$, which facilitates the high-pressure modulation of X^- excitons. We suppose that the charging effect in monolayer $MoSe_2$ is closely related with the alcohol mixture PTM.

To rationalize the charging effect and investigate the high-pressure tuning behaviors of X^0 in PL spectra, we utilized inert argon as PTM to eliminate the interference from PTM itself and obtain intrinsic features of the system. As shown in Figure 2b, the X^- and X^0 peak evolutions under pressure exhibit obviously different behaviors in the two PTM experiments. Enhancement of X^- emission is never observed in argon. Instead, it diminishes gradually with pressure, which indicates that the pressure-dependent charging effect was interdicted when PTM was replaced by argon. Therefore, emission of X^0 excitons at high pressure has been effectively tuned using argon PTM. Interestingly, a new splitting of neutral exciton X^0 emission appears above 3.7 GPa.

The PL intensity exhibits an oscillating trend as pressure increases in the alcohol mixture experiment, whereas there are monotonous decreases in the argon experiment (Figure 2a,b). In alcohol mixture PTM, the inhibitory effect of pressure on the exciton emission and the pressure-dependent charging effect together contribute to the oscillating intensity of X^- peaks, represented as the oscillation of PL intensities. However, because of blocking of the charging effect in liquid argon PTM, the intensity of exciton emission is dominated by the inhibitory effect of pressure, displaying a monotone decrease with increasing pressure. In addition, the width of peaks is observed to broaden with increasing pressure, which may be partly ascribed to the inhomogeneity of pressure arising from solidification of the pressure medium.

DOI: 10.1021/acs.jpclett.7b01374
J. Phys. Chem. Lett. 2017, 8, 3556−3563

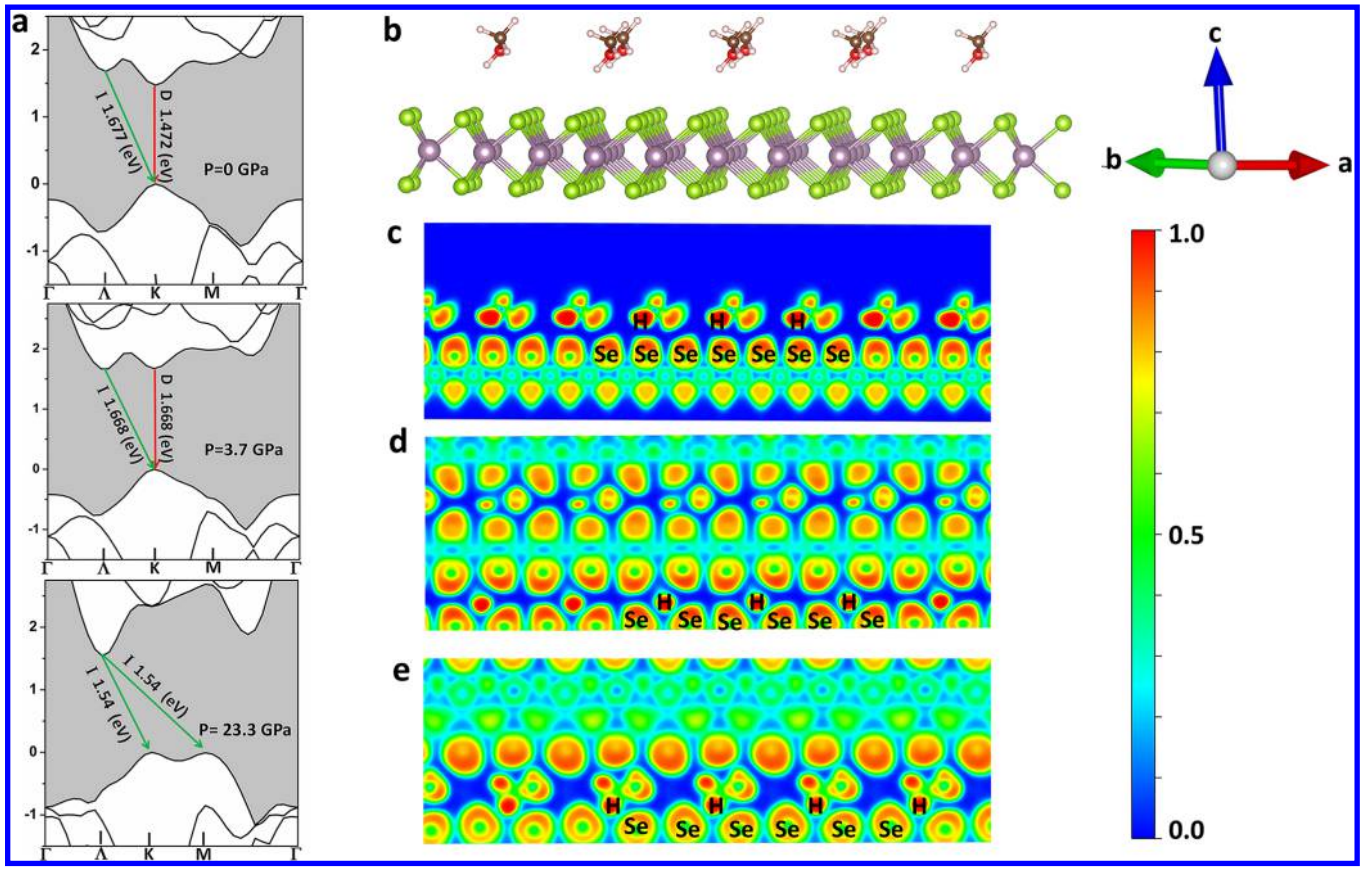

Figure 3. (a) Band structures of monolayer $MoSe_2$ at three representative pressures of 0, 3.7, and 23 GPa, depicting K−K direct interband transitions, conduction band K−Λ crossover, and valence band K−M crossover, respectively. Here, D indicates the direct band gaps and I indicates indirect band gaps. The values of D and I are also shown in the figure. (b) Calculated methanol molecule adsorption on monolayer $MoSe_2$ at 0 GPa. (c−f) ELF of the calculated structure at 0, 30, and 50 GPa.

Two opposite evolutions of area ratio of the exciton/trion (X^0/X^-) versus pressure in both PTMs are shown in Figure 2d. The area ratio of X^0/X^- declined quickly and finally disappeared with increasing pressure in the alcohol mixture PTM, while the trend of the area ratio in argon PTM was upward. These results reveal that the occurrence of the charging effect is closely related to the alcohol mixture PTM. We propose that the charging effect is derived from the interaction between H atoms of alcohol mixture PTM and Se atoms of monolayer $MoSe_2$ at high pressure, and the related DFT calculations are described in the following.

The energy evolutions of X^- and X^0 exciton emission as a function of pressure in two PTMs are illustrated in Figure 2c. In the alcohol mixture PTM experiment, the neutral exciton X^0 emission disappeared at 3.2 GPa, and a turning point in pressure evolution of negatively charged exciton X^- emission can be observed. The sectionalized linear equation, $E_g = 1.548 + 0.009P$ ($P < 3.7$ GPa) and $E_g = 1.588 + 0.001P$ ($P \geq 3.7$ GPa), fits the experimental data well. On the other hand, in argon PTM, it gives three main PL peaks, as shown by solid circles. The X^- emission (blue solid circle) diminishes and disappears after 3.7 GPa, while the X^0 emission presents a continuous blue shift with pressure up to 23.3 GPa, which is diametrically opposed to that in alcohol mixture PTM. A second-order polynomial fit $E_g = 1.589 + 0.007P - 5.867 \times 10^{-5}P^2$ can be applied to describe the pressure dependence of the main peak. After 3.7 GPa, a new split peak appears at the lower energy side and gives a pressure evolution expressed by linearly fitting $E_g = 1.618 + 7.365 \times 10^{-4}P$. Notably, the novel emerged PL emission in argon PTM and the X^- emission in alcohol mixture PTM ($P \geq 3.7$ GPa) give a similar pressure trend but with an energy discrepancy of about 30 meV. It is worth mentioning that the monolayer $MoSe_2$ in either alcohol mixture PMT or argon PMT displays discontinuous changes at 3.7 GPa, which indicates that it is a key point in the process of the hydrostatic pressure-modulated electronic band structure.

First-principles DFT calculations were employed to calculate the band structure of monolayer $MoSe_2$ with CASTAP code for a better understanding of the energy evolutions of X^- and X^0 emission during compression,[37] and the obtained results are shown in Figure 3a. At 0 GPa, the direct band gap of 1.472 eV initially lies in K−K points. Both X^0 and X^- excitons exit in K−K points, and their energy tuned by pressurization presents a trend of increase. When the pressure reaches up to 3.7 GPa, a conduction band K−Λ crossover behavior is observed, and the direct band gap of K−K points coincides with the indirect band gap of Λ−K points of 1.668 eV. The pressure value of conduction band K−Λ crossover obtained from theoretical calculation matches well with the experimental key point of 3.7 GPa. Upon further increasing the pressure, the conduction band minimum at the Λ point continues dropping and becomes much lower than that of the K point, and the monolayer $MoSe_2$ then transforms into an indirect band gap semiconductor (Figure S3). During this process, X^0 emission is divided into indirect Λ−K and direct K−K interband transitions, and the energy of X^0 existing in these two parts

DOI: 10.1021/acs.jpclett.7b01374
J. Phys. Chem. Lett. 2017, 8, 3556−3563

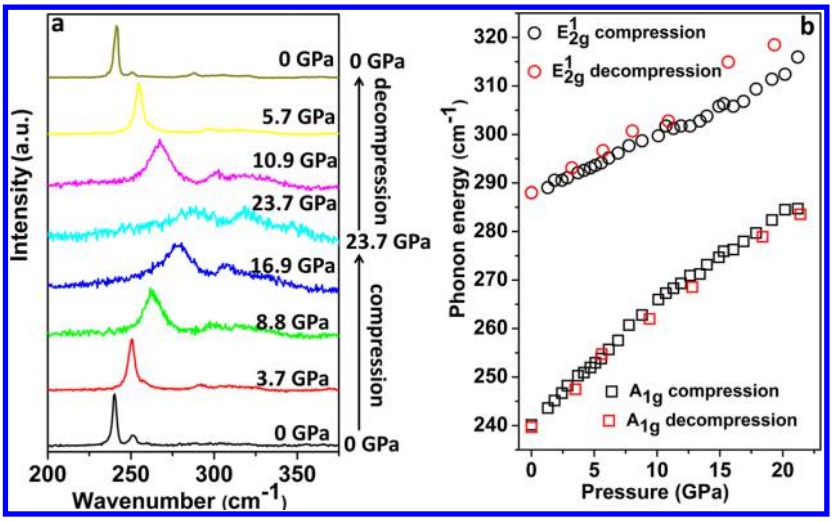

Figure 4. (a) Raman spectra of monolayer $MoSe_2$ in argon PTM during a pressure cycle. (b) Pressure dependence of Raman frequencies for A_{1g} and E_{2g}^1 modes during compression and decompression in argon PTMs.

tends to increase and remain nearly unchanged, respectively, with the pressure modulation. In the case of X^- emission, it only lies in the indirect Λ−K interband transition, and the corresponding energy shows a similar evolving model with that of X^0 located at the Λ−K interband transition. These calculated results are in good agreement with experimental phenomenon of X^0 emission splitting and X^- exciton energy reaching saturation. Up to 23.3 GPa, the indirect band gaps of Λ−K points and Λ−M points match the value of 1.54 eV. The pressure-induced valence band K−M crossover turns up, and indirect interband transition shifts from Λ−K to Λ−M points afterward (Figure 3a).

Now, the evolutions of X^- and X^0 emission are clear by combining the experimental and calculated results. Pressure-induced conduction band K−Λ crossing occurred at 3.7 GPa, which is related to its direct band gap to indirect band gap transition. For monolayer $MoSe_2$ in argon PMT, the novel emerging PL emission on the left side of the original main peak is attributed to the Λ−K interband transitions after the conduction band K−Λ crossover at 3.7 GPa, and the original main X^0 emission peak existing in the whole pressure ranges comes from K−K transitions. The fitted polynomial to the original main X^0 emission matches well with the K−K interband transitions of theoretical calculations, even though it turns from a direct band gap (before 3.7 GPa) to an indirect band gap transition due to the existence of conduction band K−Λ crossover.

For monolayer $MoSe_2$ in alcohol mixture PTM, when conduction band K−Λ crossover occurs, the blue shift of negatively charged exciton X^- emission slows down obviously above 3.7 GPa, implying that the X^- emission transitions occur in K−K points at low pressure but occur in Λ−K points at high pressure. This behavior matches with a previous report on monolayer WSe_2 that X^- emission transitions occur only in Λ−K points not in K−K points after conduction band K−Λ crossover because the ionized electrons populate the conduction band minimum to form X^- emission.[38] Besides, as we mentioned before, there is about a 30 meV energy discrepancy between the novel emerged PL emission in argon PTM and the X^- emission in alcohol mixture PTM ($P \geq 3.7$ GPa), but they possess a similar pressure trend. This is because they both come from the indirect transitions in Λ−K points after 3.7 GPa, and the 30 meV energy discrepancy is known as the trion dissociation energy. It should be noted that the conduction band K−Λ crossover phenomenon in monolayer $MoSe_2$ occurs at a smaller pressure (3.7 GPa) than that of MoS_2 (22.3 GPa),[21] indicating that the X^0 and X^- exciton emission of $MoSe_2$ is easily tuned to undergo the transformation from direct to indirect band gap transition compared with monolayer MoS_2. This might partly be ascribed to the fact that the separation of the energy difference between the conduction band minimum at K and Λ points is smaller, that is, 0.04 eV for monolayer $MoSe_2$ in comparison with 0.2 eV for monolayer MoS_2. Because the PL spectra of the monolayer 2H-MoS_2 diminish to the background noise level at pressures over 16 GPa at room temperature, the behaviors of excitons after conduction band K−Λ crossover in monolayer MoS_2 were not observed. For monolayer $MoSe_2$, the behaviors of X^0 and X^- excitons lying in indirect Λ−K interband transition were successfully observed and investigated in this work, and Figure 2c is plotted to schematically illustrate their energy variations with pressure.

The content of X^- excitons can be tuned by pressure-dependent charging effects in the surroundings of the alcohol mixture, in which the electron charge was injected into alcohol-immersed $MoSe_2$ to form X^- excitons by interaction between H atoms of PTM and Se atoms of monolayer $MoSe_2$ at high pressure. This mechanism of charging effects is verified by DFT calculations performed with the VASP code.[39] As shown in Figure 3b, we place methanol molecules on the surface of monolayer $MoSe_2$ and relax the atomic structure until stable configurations are found. We calculated the electron localization function (ELF) for this atomic structure. Then, the structure was regarded as the crystal structure of a bulk material to obtain a uniform pressure from all directions. The electron with an ELF value close to 0.5 is regarded as a free electron. As shown in Figure 3c, at 0 GPa, the free electrons of H atoms in methanol molecules and Se atoms are isolated. When a pressure of 30 GPa was applied to the atomic structure from all directions, a union of free electrons derived from H and Se atoms was formed (Figure 3d). Further increasing the pressure to 50 GPa, the union of the free electrons was further strengthened due to the pressurizing-induced declination of interaction distance (Figure 3e). Despite the fact that the

DOI: 10.1021/acs.jpclett.7b01374
J. Phys. Chem. Lett. 2017, 8, 3556−3563

theoretical model could not exactly simulate the complex system of the alcohol mixture-immersed sample, it still convincingly reveals the mechanism of the charging effect and the enhanced trend during compression observed in the experiment. When the PTM was replaced by argon, the pressure-dependent charging effect was interdicted because inert properties blocked the interaction between the sample and PTM. The calculated simulation of the pressure-induced charging effect provides an excellent strategy for achieving controllable modulation of excitons and trions in 2D TMDs at extreme environments.

Another important property of monolayer $MoSe_2$ is the behavior of lattice vibrations under high pressure. We also investigate the Raman spectra of monolayer $MoSe_2$ at high pressures employing alcohol mixture and argon as PTM. Figure 4a displays a series of Raman spectra with different pressure coefficients obtained in argon PTM, in which Raman peaks exhibits a blue shift with the pressure increasing up to 23.7 GPa. Figure 4b reveals that the pressure-induced evolutions of A_{1g} and $E_{2g}{}^1$ modes are reversible, and the resulting blue shifts from 0 to 23.7 GPa are 44.6 and 28 cm^{-1}, respectively. Altering PTM with the alcohol mixture, the obtained Raman spectra did not present any observable disparity (Figure S4), which suggests that a change of PTM has a slight influence on the pressure-dependent lattice vibrations. Therefore, we conclude that the Raman mode shift based on the diamond substrate exhibits uniform change, offering a continuous excitonic tuning process upon pressurizing for the following PL measurement. In addition, a control experiment was performed by altering diamond with a Si/SiO_2 substrate, and the results are exhibited in Figure S5. The occurrence of a nonuniform Raman mode shift and softening phenomenon observed from the SiO_2/Si substrate-based experiment was supposed to be related to unit cell reduction and phase transition of the Si/SiO_2 substrate at high pressure. This nonuniform change in the volume largely limits the energy tunability of excitons and trions for potential optoelectronic applications. Therefore, we are convinced that diamond is the appropriate choice of window material for high-pressure experiments due to its outstanding resistance to pressure. In addition, using diamond as the substrate is of benefit to the optical measurements in the transmission mode and largely improves the pressure that samples could achieve, which may significantly advance the study on pressure-induced semiconducting to metallic transition in few-layered TMDs.

In conclusion, we investigated the tuning process of X^0 and X^- exciton emission by hydrostatic pressure and charging effects through PL spectra. Samples were transferred into a DAC and immersed in two kinds of PTM including a standard mixture of (4:1) methanol/ethanol and argon. Using diamond as the substrate, monolayer $MoSe_2$ shows different evolutions of pressure-dependent PL spectra in two PTMs. The content of charged exciton X^- emission increases dramatically in the alcohol mixture PTM-based experiment during compression. When the pressure goes up to the key point of 3.7 GPa, only indirect $\Lambda-K$ transition-related X^- emission is observed in the alcohol mixture experiment. In contrast, in the argon experiment, the content of charged exciton X^- emission decreases and the X^0 emission corresponding to direct $K-K$ transition and indirect $\Lambda-K$ transition is observed at 3.7 GPa and above. Moreover, theoretical calculation, consistent with the experimental results, helps us to analyze the behaviors of the exciton in PL spectra during recompression. The result of DFT calculations with VASP code reveals that the pressure-dependent charging effect observed in the alcohol mixture PTM experiment is induced by the interaction between H atoms of PTMs and Se atoms at high pressure.

EXPREIMENTAL METHODS

Sample Preparation and Characterizations. Monolayer 2H-$MoSe_2$ film was obtained from a $MoSe_2$ single crystal (2D Semiconductor Supplies, USA) by mechanical exfoliation technology on GEL film (Gel-Pak).[25,26] Afterward, the monolayer $MoSe_2$ was transferred onto a diamond anvil surface serving as the substrate in the sample chamber. A symmetric DAC with a pair of 300 μm culet anvils was used for the high-pressure experiments. A T301 stainless steel gasket with an initial thickness of 250 μm was preindented to 50 μm thick and was subsequently drilled in the center to form a hole 120 μm in diameter. The pressure of the sample chamber in DAC was measured by collecting ruby fluorescence spectra from ruby spheres loaded in the chamber.[40] The PTM, either a standard mixture of (4:1) methanol/ethanol or argon, was also loaded in the sample chamber to provide a hydrostatic pressure condition for the samples.

Raman, PL spectroscopy, and optical contrast were used to determine the layers of $MoSe_2$. Raman and PL measurements were conducted using a micro-Raman spectrometer (Horiba-JY T64000) equipped with a solid-state green laser (λ = 532 nm) in a backscattering configuration. The signals were dispersed by an 1800 g mm^{-1} (Raman) and a 600 g mm^{-1} (PL) grating and collected via a 50× objective lens under atmospheric conditions and high pressures, respectively. Considering the probable damage from heating or oxidizing under exposure, the estimated laser power at the surface of the sample was set to be less than 0.5 mW.

Theoretical Calculations. The first-principles calculations based on DFT were performed to provide insight into the energy band of monolayer $MoSe_2$ at high pressure. Perdew–Burke–Ernzerh (PBE) of generalized gradient approximation (GGA) functional with the exchange–correlation functional and norm-conserving was used as the type of pseudopotential during the whole computational procedure. Calculation of the energy band was performed with a plane-wave cutoff energy of 800 eV and a K-point set of 18 × 18 × 1. A 20 Å vacuum spacing was set as the interatomic spacing to avoid artificial couplings between adjacent atomic layers. The self-consistent field (SCF) was managed to be less than 5×10^{-7} eV/atom to ensure the accuracy of calculated results. The band structure of monolayer $MoSe_2$ can be calculated via the modulated lattice parameter a at selected pressures obtained by applying the procedure of geometry optimization. All of the calculations were performed in the CASTEP code.

The stable structure of methanol molecule adsorption on monolayer $MoSe_2$ was obtained using DFT within the PBE of parametrization of the GGA, as implemented in the Vienna ab initio simulation package VASP code. A 20 Å vacuum spacing was set as the interatomic spacing to acquire the stable structure at 0 GPa. Then, the structure was regarded as the crystal structure of a bulk material to obtain the uniform pressure from all directions. A plane-wave cutoff energy of 900 eV was sufficient for the initial search over structures. The ELF calculations were introduced to analyze the behaviors of free electrons existing in H and Se atoms. A well-converged Monkhorst–Pack k point set of 5 × 5 × 1 was used for this procedure.

DOI: 10.1021/acs.jpclett.7b01374
J. Phys. Chem. Lett. 2017, 8, 3556–3563

■ ASSOCIATED CONTENT

Supporting Information

The Supporting Information is available free of charge on the ACS Publications website at DOI: 10.1021/acs.jpclett.7b01374.

Photo of the monolayer $MoSe_2$ on a diamond substrate in liquid argon PTM; Raman spectrum of bulk 2H-$MoSe_2$ at ambient conditions; band structures of monolayer $MoSe_2$ at representative pressures; comparison of Raman in two PTMs; comparison of Raman on diamond and SiO_2/Si substrates (PDF)

■ AUTHOR INFORMATION

Corresponding Authors

*E-mail: lifangfei@jlu.edu.cn (F.L.).
*E-mail: zhouqiang@jlu.edu.cn (Q.Z.).

ORCID

Fangfei Li: 0000-0002-0342-3872
Tian Cui: 0000-0002-9664-848X

Notes

The authors declare no competing financial interest.

■ ACKNOWLEDGMENTS

The authors are grateful to Sergey N. Tkachev for his help loading the argon PTM. Use of the COMPRES-GSECARS gas loading system was supported by COMPRES under NSF Cooperative Agreement EAR -1606856 and by GSECARS through NSF grant EAR-1634415 and DOE grant DE-FG02-94ER14466. This research used resources of the Advanced Photon Source, a U.S. Department of Energy (DOE) Office of Science User Facility operated for the DOE Office of Science by Argonne National Laboratory under Contract No. DE-AC02-06CH11357. This work was supported by the National Natural Science Foundation of China (Nos. 11574112, 11474127, 11274137), National Basic Research Program of China (No. 2011CB808200), Program for Changjiang Scholars and Innovative Research Team in University (No. IRT1132), and China Postdoctoral Science Foundation (2015M570265).

■ REFERENCES

(1) Cao, T.; Wang, G.; Han, W.; Ye, H.; Zhu, C.; Shi, J.; Niu, Q.; Tan, P.; Wang, E.; Liu, B.; Feng, J. Valley-Selective Circular Dichroism of Monolayer Molybdenum Disulphide. *Nat. Commun.* **2012**, *3*, 887.

(2) Allain, A.; Kis, A. Electron and Hole Mobilities in Single-Layer WSe_2. *ACS Nano* **2014**, *8*, 7180−7185.

(3) Mak, K. F.; He, K.; Shan, J.; Heinz, T. F. Control of Valley Polarization in Monolayer MoS_2 by Optical Helicity. *Nat. Nanotechnol.* **2012**, *7*, 494−498.

(4) Zeng, H. L.; Dai, J. F.; Yao, W.; Xiao, D.; Cui, X. D. Valley Polarization in MoS_2 Monolayers by Optical Pumping. *Nat. Nanotechnol.* **2012**, *7*, 490−493.

(5) Ganatra, R.; Zhang, Q. Few-Layer MoS_2: A Promising Layered Semiconductor. *ACS Nano* **2014**, *8*, 4074−4099.

(6) Dou, X. M.; Ding, K.; Jiang, D. S.; Fan, X. F.; Sun, B. Q. Probing Spin-Orbit Coupling and Interlayer Coupling in Atomically Thin Molybdenum Disulfide Using Hydrostatic Pressure. *ACS Nano* **2016**, *10*, 1619−1624.

(7) Ross, J. S.; Wu, S. F.; Yu, H. Y.; Ghimire, N. J.; Jones, A. M.; Aivazian, G.; Yan, J. Q.; Mandrus, D. G.; Xiao, D.; Yao, W.; Xu, X. D. Electrical Control of Neutral and Charged Excitons in a Monolayer Semiconductor. *Nat. Commun.* **2013**, *4*, 1474.

(8) Singh, A.; Moody, G.; Wu, S.; Wu, Y.; Ghimire, N. J.; Yan, J.; Mandrus, D. G.; Xu, X.; Li, X. Coherent Electronic Coupling in Atomically Thin $MoSe_2$. *Phys. Rev. Lett.* **2014**, *112*, 216804.

(9) Mak, K. F.; He, K. L.; Lee, C.; Lee, G. H.; Hone, J.; Heinz, T. F.; Shan, J. Tightly Bound Trions in Monolayer MoS_2. *Nat. Mater.* **2012**, *12*, 207−211.

(10) Jones, A. M.; Yu, H.; Ghimire, N. J.; Wu, S.; Aivazian, G.; Ross, J. S.; Zhao, B.; Yan, J.; Mandrus, D. G.; Xiao, D.; Yao, W.; Xu, X. Optical Generation of Excitonic Valley Coherence in Monolayer WSe_2. *Nat. Nanotechnol.* **2013**, *8*, 634−638.

(11) Pospischil, A.; Furchi, M. M.; Mueller, T. Solar-Energy Conversion and Light Emission in an Atomic Monolayer p-n Diode. *Nat. Nanotechnol.* **2014**, *9*, 257−261.

(12) Ganatra, R.; Zhang, Q. Few-Layer MoS_2: A Promising Layered Semiconductor. *ACS Nano* **2014**, *8*, 4074−4099.

(13) Xia, F. N.; Wang, H.; Xiao, D.; Dubey, M.; Ramasubramaniam, A. Two-Dimensional Material Nanophotonics. *Nat. Photonics* **2014**, *8*, 899−907.

(14) Baugher, B. W. H.; Churchill, H. O. H.; Yang, Y. F.; Jarillo-Herrero, P. Optoelectronic Devices Based on Electrically Tunable p-n Diodes in a Monolayer Dichalcogenide. *Nat. Nanotechnol.* **2014**, *9*, 262−267.

(15) Lopez-Sanchez, O.; Lembke, D.; Kayci, M.; Radenovic, A.; Kis, A. Ultrasensitive Photodetectors Based on Monolayer MoS_2. *Nat. Nanotechnol.* **2013**, *8*, 497−501.

(16) Sim, S.; Park, J.; Song, J. G.; In, C.; Lee, Y. S.; Kim, H.; Choi, H. Exciton Dynamics in Atomically Thin MoS_2: Interexcitonic Interaction and Broadening Kinetics. *Phys. Rev. B: Condens. Matter Mater. Phys.* **2013**, *88*, 075434.

(17) Wang, R.; Ruzicka, B. A.; Kumar, N.; Bellus, M. Z.; Chiu, H. Y.; Zhao, H. Ultrafast and Spatially Resolved Studies of Charge Carriers in Atomically Thin Molybdenum Disulfide. *Phys. Rev. B: Condens. Matter Mater. Phys.* **2012**, *86*, 045406.

(18) Shi, H. Y.; Yan, R. S.; Bertolazzi, S.; Brivio, J.; Gao, B.; Kis, A.; Jena, D.; Xing, H. G.; Huang, L. B. Exciton Dynamics in Suspended Mono layer and Few-Layer MoS_2 2D Crystals. *ACS Nano* **2013**, *7*, 1072−1080.

(19) Sie, E. J.; Frenzel, A. J.; Lee, Y. H.; Kong, J.; Gedik, N. Intervalley Biexcitons and Many-Body Effects in Monolayer MoS_2. *Phys. Rev. B: Condens. Matter Mater. Phys.* **2015**, *92*, 125417.

(20) Mai, C.; Barrette, A.; Yu, Y. F.; Semenov, Y. G.; Kim, K. W.; Cao, L. Y.; Gundogdu, K. Many-Body Effects in Valleytronics: Direct Measurement of Valley Lifetimes in Single-Layer MoS_2. *Nano Lett.* **2014**, *14*, 202−206.

(21) Nayak, A. P.; Pandey, T.; Voiry, D.; Liu, J.; Moran, S. T.; Sharma, A.; Tan, C.; Chen, C. H.; Li, L. J.; Chhowalla, M.; Lin, J. F.; Singh, A. K.; Akinwande, D. Pressure-Dependent Optical and Vibrational Properties of Monolayer Molybdenum Disulfide. *Nano Lett.* **2015**, *15*, 346−353.

(22) Pandey, T.; et al. Pressure-Induced Charge Transfer Doping of Monolayer Graphene/MoS2 Heterostructure. *Small* **2016**, *12*, 4063−4069.

(23) Ross, J. S.; Klement, P.; et al. Electrically Tunable Excitonic Light-Emitting Diodes Based on Monolayer WSe_2 p-n Junctions. *Nat. Nanotechnol.* **2014**, *9*, 268−272.

(24) Jo, S.; Ubrig, N.; Berger, H.; Kuzmenko, A. B.; Morpurgo, A. F. Mono- and Bilayer WS_2 Light-Emitting Transistors. *Nano Lett.* **2014**, *14*, 2019−2025.

(25) Castellanos-Gomez, A.; Buscema, M.; Molenaar, R.; Singh, V.; Janssen, L.; van der Zant, H. S. J.; Steele, G. A. Deterministic Transfer of Two-Dimensional Materials by All-Dry Viscoelastic Stamping. *2D Mater.* **2014**, *1*, 011002.

(26) Castellanos-Gomez, A.; Vicarelli, L.; Prada, E.; Island, J. O.; Narasimha-Acharya, K. L.; Blanter, S. I.; Groenendijk, D. J.; Buscema, M.; Steele, G. A.; Alvarez, J. V.; Zandbergen, H. W.; Palacios, J. J.; van der Zant, H. S. J. Isolation and Characterization of Few-Layer Black Phosphorus. *2D Mater.* **2014**, *1*, 025001.

(27) Tonndorf, P.; Schmidt, R.; Bottger, P.; Zhang, X.; Borner, J.; Liebig, A.; Albrecht, M.; Kloc, C.; Gordan, O.; Zahn, D. R. T.; Michaelis de Vasconcellos, S.; Bratschitsch, R. Photoluminescence Emission and Raman Response of Monolayer MoS_2, $MoSe_2$, and WSe_2. *Opt. Express* **2013**, *21*, 4908−4916.

DOI: 10.1021/acs.jpclett.7b01374
J. Phys. Chem. Lett. 2017, 8, 3556−3563

(28) Lu, X.; Utama, M. I. B.; Lin, J. H.; Gong, X.; Zhang, J.; Zhao, Y. Y.; Pantelides, S. T.; Wang, J. X.; Dong, Z. L.; Liu, Z.; Zhou, W.; Xiong, Q. H. Large-Area Synthesis of Monolayer and Few-Layer $MoSe_2$ Films on SiO_2 Substrates. *Nano Lett.* **2014**, *14*, 2419−2425.
(29) Tongay, S.; Suh, J.; Ataca, C.; Fan, W.; Luce, A.; Kang, J. S.; Liu, J.; Ko, C.; Raghunathanan, R.; Zhou, J.; Ogletree, F.; Li, J. B.; Grossman, J. C.; Wu, J. Q. Defects Activated Photoluminescence in Two-Dimensional Semiconductors: Interplay Between Bound, Charged, and Free Excitons. *Sci. Rep.* **2013**, *3*, 2657.
(30) Shim, G. W.; Yoo, K.; Seo, S. B.; Shin, J.; Jung, D. Y.; Kang, I. S.; Ahn, C. W.; Cho, B. J.; Choi, S. Y. Large-Area Single-Layer $MoSe_2$ and Its van der Waals Heterostructures. *ACS Nano* **2014**, *8*, 6655−6662.
(31) Zhou, W.; Zou, X. L.; Najmaei, S.; Liu, Z.; Shi, Y. M.; Kong, J.; Lou, J.; Ajayan, P. M.; Yakobson, B. I.; Idrobo, J. C. Intrinsic Structural Defects in Monolayer Molybdenum Disulfide. *Nano Lett.* **2013**, *13*, 2615−2622.
(32) Elias, A. L.; Perea-Lopez, N.; Castro-Beltran, A.; Berkdemir, A.; Lv, R. T.; Feng, S. M.; Long, A. D.; Hayashi, T.; Kim, Y. A.; Endo, M.; et al. Controlled Synthesis and Transfer of Large-Area WS_2 Sheets: From Single Layer to Few Layers. *ACS Nano* **2013**, *7*, 5235−5242.
(33) Peimyoo, N.; Shang, J. Z.; Cong, C. X.; Shen, X. N.; Wu, X. Y.; Yeow, E. K. L.; Yu, T. Nonblinking, Intense Two-Dimensional Light Emitter: Mono Layer WS_2 Triangles. *ACS Nano* **2013**, *7*, 10985−10994.
(34) Luo, X.; Zhao, Y. Y.; Zhang, J.; Xiong, Q. H.; Quek, S. Y. Anomalous Frequency Trends in MoS_2 Thin Films Attributed to Surface Effects. *Phys. Rev. B: Condens. Matter Mater. Phys.* **2013**, *88*, 075320.
(35) Lee, C.; Yan, H.; Brus, L. E.; Heinz, T. F.; Hone, J.; Ryu, S. Anomalous Lattice Vibrations of Single- and Few-Layer MoS_2. *ACS Nano* **2010**, *4*, 2695−2700.
(36) Lu, X.; Utama, M. I. B.; Lin, J. H.; Luo, X.; Zhao, Y. Y.; Zhang, J.; Pantelides, S. T.; Zhou, W.; Quek, S. Y.; Xiong, Q. H. Rapid and Nondestructive Identification of Polytypism and Stacking Sequences in Few-Layer Molybdenum Diselenide by Raman Spectroscopy. *Adv. Mater.* **2015**, *27*, 4502−4508.
(37) Ye, Y. X.; Dou, X. M.; Ding, K.; Jiang, D. S.; Yang, F. H.; Sun, B. Q. Pressure-Induced K-Λ Crossing in Monolayer WSe_2. *Nanoscale* **2016**, *8*, 10843−10848.
(38) Perdew, J. P.; Burke, K.; Ernzerhof, M. Generalized Gradient Approximation Made Simple. *Phys. Rev. Lett.* **1996**, *77*, 3865−3868.
(39) Kresse, G.; Furthmüller, J. Efficiency of Ab-Initio Total Energy Calculations for Metals and Semiconductors Using a Plane-Wave Basis Set. *Comput. Mater. Sci.* **1996**, *6*, 15−50.
(40) Mao, H. K.; Xu, J.; Bell, P. M. Calibration of the Ruby Pressure Gauge to 800 kbar Under Quasi-Hydrostatic Conditions. *J. Geophys. Res.* **1986**, *91*, 4673−4676.

DOI: 10.1021/acs.jpclett.7b01374
J. Phys. Chem. Lett. 2017, 8, 3556−3563